Theoretical Analysis of Microwave Heating of Dielectric Materials Filled in a Rectangular Waveguide With Various Resonator Distances

Phadungsak Rattanadecho
e-mail: ratphadu@engr.tu.ac.th

Waraporn Klinbun

Research Center of Microwave Utilization in Engineering (RCME),
Department of Mechanical Engineering,
Faculty of Engineering,
Thammasat University (Rangsit Campus),
Pathumthani 12120, Thailand

This paper proposes mathematical models of the microwave heating process of dielectric materials filled in a rectangular waveguide with a resonator. A microwave system supplies a monochromatic wave in a fundamental mode (TE_{10} mode). A convection exchange at the upper surface of the sample is considered. The effects of resonator distance and operating frequency on distributions of electromagnetic fields inside the waveguide, temperature profile, and flow pattern within the sample are investigated. The finite-difference time-domain method is used to determine the electromagnetic field distribution in a microwave cavity by solving the transient Maxwell equations. The finite control volume method based on the SIMPLE *algorithm is used to predict the heat transfer and fluid flow model. Two dielectric materials, saturated porous medium and water, are chosen to display microwave heating phenomena. The simulation results agree well with the experimental data. Based on the results obtained, the inserted resonator has a strong effect on the uniformity of temperature distributions, depending on the penetration depth of microwave. The optimum distances of the resonator depend greatly on the operating frequencies.* [DOI: 10.1115/1.4002628]

Keywords: microwave heating, rectangular waveguide, TE_{10} mode, porous medium, resonator

1 Introduction

AQ: #1 Microwave is a form of electromagnetic wave with wavelengths ranging from 1 m down to 1 mm, with frequencies between 0.3 GHz and 300 GHz. Microwave is applied in many industry and household as a source of thermal energy. It is used in the drying of textile, paper, photographic film, and leather. Other uses include vulcanization, casting, and cross-linking polymers. Perhaps, the largest consumer of microwave power is the food industry, where it is used for cooking, thawing, freeze drying, sterilization, pasteurization, etc. This is the result of the energy carried by the microwave that is converted to thermal energy within the material and a very rapid temperature increase throughout the material that may lead to less by-products and decomposition products. In addition, microwave heating has several advantages, such as high speed startup, selective energy absorption, instantaneous electric control, nonpollution, high energy efficiency, and high product quality.

In order to maintain product quality, uniform distribution of heat is of paramount importance in these processes. The factors that influence the uniformity of heat are load factors and microwave system factors. For example, dielectric properties, volume, shape, and mixture ratio are load factors [1]. Microwave system factors are turntable, operating frequency, placement inside the oven, oven size, and geometry [2]. Knowledge of several parameters is required for an accurate account of all phenomena that occur in a dielectric heated by microwaves. This includes a description of electromagnetic field distribution, power absorbed, temperature, and velocity field. For this reason, we need to solve Maxwell's equation, momentum, and energy equation. Since the complexity and number of the equations are involved, a numerical method is the only approach to conduct realistic process simulations.

The computational study interactions between electromagnetic field and dielectric materials have been investigated in a variety of microwave applicator, such as a multimode cavity (Datta et al. [3], Jia and Bialkowski [4], Lui et al. [5], Ayappa et al. [6], Zhang et al. [7], Clemens and Saltiel [8], Chatterjee et al. [9], and Zhu et al. [10–13]) and a rectangular waveguide (Ratanedecho et al. [14–16], Rattanedecho [17], Curet et al. [18], and Tada et al. [19]). The dielectric materials, such as food, liquid, and a saturated porous packed bed, are chosen for investigating microwave heating phenomena. Ratanedecho et al. [15] investigated, both numerically and experimentally, the microwave heating of a liquid sample in a rectangular waveguide. Microwave was operated in TE_{10} mode at a frequency of 2.45 GHz. The movement of liquid induced by microwave energy was taken into account. Coupled electromagnetic, flow field, and thermal profile were simulated in two-dimensional. Their work showed the effects of liquid electric conductivity and microwave power level on the degree of penetration and rate of heat generation within a liquid layer. Results showed that the heating kinetic strongly depends on the dielectric properties. Ratanedecho et al. [16] investigated the heating of multilayered materials by microwave heating with a rectangular waveguide. They found that when a layer of lower dielectric material is attached in front of a sample, the microwave energy absorbed and the distribution of temperature within the sample are enhanced. Basak et al. [20] studied the efficient microwave heating of porous dielectrics. The results showed that the average power absorption of the samples (b/a and b/o) was enhanced in the presence of Al_2O_3 support. Thermal runaway heating was ob-

Contributed by the Heat Transfer Division of ASME for publication in the JOURNAL OF HEAT TRANSFER. Manuscript received September 14, 2010; final manuscript received September 26, 2010; published online xxxxx-xxxxx-xxxxx. Assoc. Editor: Yogesh Jaluria.

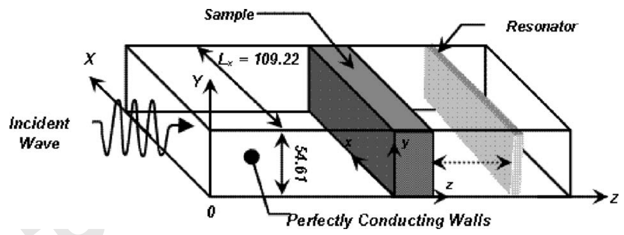

Fig. 1 Schematic of microwave system

served at the face that was not attached with support for the b/a sample and the intensity of thermal runaway increase with porosity, whereas lower thermal runaway was observed for b/o samples at all porosity values. The last, one side incidence may correspond to the largest heating rates, whereas distributed sources may correspond to smaller thermal runaway for both samples.

Many parameters, such as dielectric properties, sample volume, microwave power level, turntable, and operating frequency, were studied in detail. Rattanadecho [17] developed two-dimensional models to predict the electromagnetic fields (TE_{10} mode) inside a guide and the power and temperature distributions within a wood located in a rectangular waveguide. His simulations were performed showing the influence of irradiation times, working frequencies, and sample size. Chatterjee et al. [9] numerically investigated the heating of containerized liquid using microwave radiation. The effects of turntable rotation, natural convection, power source, and aspect ratio of container on the temperature profile were studied, and they presented detailed results of temperature profiles, stream functions, and time evolution of flow field. Results indicated that turntable rotation did not aid in achieving uniform heating in the case of a symmetric heat source. Zhu et al. [10,11] presented a numerical model to study heat transfer in liquids that flowed continuously in a circular duct that was subjected to microwave heating. The results showed that the heating pattern strongly depends on the dielectric properties of the fluid in the duct and on the geometry of the microwave heating system.

However, the effects of the operating frequency and resonator distance on microwave phenomena in the case of using a rectangular waveguide with a resonator have not been clearly studied yet. The present study concerns with a microwave heating of the dielectric materials subjected to a monochromatic wave (TE_{10} mode). The objective of this study can be summarized by the following items: (i) A two-dimensional microwave heating model is carried out to predict the distribution of electromagnetic fields, temperatures, and velocities. (ii) Simulation results are compared and validated with the experimental results in previous works. (iii) The effects of resonator, resonator distances (0 mm, 50 mm, 100 mm, and 200 mm), operating frequencies (1.5 GHz, 2.45 GHz, and 5.8 GHz), and dielectric properties microwave heating phenomena are studied.

2 Problem Description

Figure 1 depicts the physical model of the problem. It is a microwave system supplying a monochromatic wave in the fundamental mode (TE_{10} mode). Microwave energy is transmitted along the Z-direction of a rectangular waveguide (cross section area of $109.2\times 54.6\ \text{mm}^2$) with microwave power input of 300 W. The walls of the guide are thermally insulated and are perfect electric conductors. A resonator inserted at the end of the guide is used to reflect a transmitted wave, and resonator distances are referred to distances between the bottom surface of the sample and the surface of the resonator. The sample (cross section area of $109.2\times 54.6\ \text{mm}^2$) fills the guide. The upper surface of the sample is exposed for a convection exchange with ambient temperature. The samples are saturated porous medium and water. A saturated porous medium is a packed bed consisting of single sized glass beads with voids filled with water. The porosity of the medium is 0.385 everywhere. The coordinate system designated by XYZ is used to describe electromagnetic fields, and the system, xyz, is designated for describing the temperature and flow fields.

3 Modeling of Microwave Heating

3.1 Modeling of Electromagnetic Fields. The electromagnetic field is solved according to the theory of Maxwell's equations. In this study, we consider in a fundamental mode (TE_{10}), therefore, Maxwell's equations in terms of the electric and magnetic intensities given by Ratanedecho et al. [15],

$$\varepsilon\frac{\partial E_Y}{\partial t}=\frac{\partial H_X}{\partial Z}-\frac{\partial H_Z}{\partial X}-\sigma E_Y \tag{1}$$

$$\mu\frac{\partial H_Z}{\partial t}=-\frac{\partial E_Y}{\partial X} \tag{2}$$

$$\mu\frac{\partial H_X}{\partial t}=\frac{\partial E_Y}{\partial Z} \tag{3}$$

where

$$\varepsilon=\varepsilon_0\varepsilon_r,\quad \mu=\mu_0\mu_r,\quad \sigma=2\pi f\varepsilon\tan\delta \tag{4}$$

ε is the complex permittivity, σ is the electrical conductivity, and μ is the magnetic permeability. In addition, if magnetic effects are negligible, which is proven to be a valid assumption for most dielectric materials used in microwave heating applications, the magnetic permeability (μ) is well approximated by its value (μ_0) in the free space. tan δ is the loss tangent coefficient.

In this study, dielectric properties of samples depend on temperature as follows:

$$\varepsilon_r(T)=\varepsilon_r'(T)-j\varepsilon_r''(T) \tag{5}$$

where

$$\varepsilon_r'(T)=\phi\varepsilon_{rw}'(T)+(1-\phi)\varepsilon_{rp}'(T) \tag{6}$$

$$\varepsilon_r''(T)=\phi\varepsilon_{rw}''(T)+(1-\phi)\varepsilon_{rp}''(T) \tag{7}$$

ϕ is the porosity, thus, a case of water $\phi=1$,

$$\tan\delta=\frac{\varepsilon_r''(T)}{\varepsilon_r'(T)} \tag{8}$$

From the Poynting vector, the volumetric power absorbed (Q) by a dielectric material can be calculated from the local electric fields [15]:

$$Q=2\pi f\varepsilon_0\varepsilon_r'(\tan\delta)\cdot E_Y^2 \tag{9}$$

3.2 Boundary Conditions. The upper surface of the sample is partially received incident electromagnetic wave and the sidewalls of the waveguide are perfect electric conductors.

1. *Perfectly conducting boundary*: Boundary conditions on the inner wall surface of waveguide and at resonator are given by Faraday's law and Gauss's theorem [15]:

$$E_t=0,\quad H_n=0 \tag{10}$$

where t and n denote tangential and normal components, respectively.

2. *Continuity boundary condition*: Boundary conditions along the interface between the sample and air are given by Ampere's law and Gauss's theorem [15]:

$$E_t=E_t',\quad H_t=H_t'$$

$$D_n=D_n',\quad B_n=B_b' \tag{11}$$

3. *Absorbing boundary condition*: At both ends of rectangular

waveguide, the first-order absorbing conditions are applied [15]:

$$\frac{\partial E_Y}{\partial t} = \pm \upsilon \frac{\partial E_Y}{\partial Z} \tag{12}$$

where $\pm$ is represented as the forward and backward directions and υ is the velocity of wave propagation.

4. *Oscillation of the electric and magnetic intensities by magnetron*: An incident wave due to magnetron is given by Ratanedecho et al. [15],

$$E_Y = E_{Yin} \sin\left(\frac{\pi X}{L_X}\right)\sin(2\pi f t) \tag{13}$$

$$H_X = \frac{E_{Yin}}{Z_H}\sin\left(\frac{\pi X}{L_X}\right)\sin(2\pi f t) \tag{14}$$

where E_{Yin} is the input value of electric fields intensity, L_X is the length of the rectangular waveguide in the X-direction, and Z_H is the wave impedance defined as follows:

$$Z_H = \frac{\lambda_g Z_I}{\lambda} = \frac{\lambda_g}{\lambda}\sqrt{\frac{\mu}{\varepsilon}} \tag{15}$$

Here, Z_I is the intrinsic impedance depending on the properties of the material, and λ and λ_g are the wavelengths of microwave in free space and rectangular waveguide, respectively.

3.3 Modeling of Heat Transfer and Fluid Flow. To reduce the complexity of the problem, the following assumptions have been introduced into energy and fluid flow equations, particularly in the case of the saturated porous packed bed sample:

1. The saturated fluid within the medium is in a local thermodynamic equilibrium with the solid matrix.
2. The saturated porous packed bed is rigid and no chemical reactions occur.
3. The fluid flow is unsteady, laminar, and incompressible.
4. The pressure work and viscous dissipation are all assumed negligible.
5. The solid matrix is made of spherical particles while the porosity and permeability of the medium are assumed to be uniform throughout the saturated porous packed bed.
6. There is no phase change for the liquid and solid phases.
7. The samples are homogeneous and isotropic.

Heat equation: For saturated porous packed bed and water layer, as follows [21]:

$$\Phi\frac{\partial T}{\partial t} + u\frac{\partial T}{\partial x} + w\frac{\partial T}{\partial z} = \alpha\left(\frac{\partial^2 T}{\partial x^2} + \frac{\partial^2 T}{\partial z^2}\right) + \frac{Q}{(\rho C_p)_w} \tag{16}$$

$\Phi = [\phi(\rho C_p)_w + (1-\phi)(\rho C_p)_p]/(\rho C_p)_w$ is the heat capacity ratio. If the sample is water, the heat capacity ratio has a value of 1. Q is the volumetric power absorbed, which is calculated from Eq. (9).

Continuity equation:

$$\frac{\partial u}{\partial x} + \frac{\partial w}{\partial z} = 0 \tag{17}$$

Momentum equations:

1. For water layer [15]:

$$\frac{\partial u}{\partial t} + \frac{\partial (u\cdot u)}{\partial x} + \frac{\partial (w\cdot u)}{\partial z} = -\frac{1}{\rho_w}\frac{\partial P}{\partial x} + \nu\left(\frac{\partial^2 u}{\partial x^2} + \frac{\partial^2 u}{\partial z^2}\right) \tag{18}$$

$$\frac{\partial w}{\partial t} + \frac{\partial (u\cdot w)}{\partial x} + \frac{\partial (w\cdot w)}{\partial z} = -\frac{1}{\rho_w}\frac{\partial P}{\partial z} + \nu\left(\frac{\partial^2 w}{\partial x^2} + \frac{\partial^2 w}{\partial z^2}\right) + g\beta(T - T_\infty) \tag{19}$$

2. For saturated porous packed bed [21]:

$$\frac{1}{\phi}\frac{\partial u}{\partial t} + \frac{1}{\phi^2}\frac{\partial (u\cdot u)}{\partial x} + \frac{1}{\phi^2}\frac{\partial (w\cdot u)}{\partial z} = -\frac{1}{\rho_w}\frac{\partial P}{\partial x} + \frac{\nu}{\phi}\left(\frac{\partial^2 u}{\partial x^2} + \frac{\partial^2 u}{\partial z^2}\right) - \frac{\gamma u}{\rho_w \mathrm{K}} \tag{20}$$

$$\frac{1}{\phi}\frac{\partial w}{\partial t} + \frac{1}{\phi^2}\frac{\partial (u\cdot w)}{\partial x} + \frac{1}{\phi^2}\frac{\partial (w\cdot w)}{\partial z} = -\frac{1}{\rho_w}\frac{\partial P}{\partial z} + \frac{\nu}{\phi}\left(\frac{\partial^2 w}{\partial x^2} + \frac{\partial^2 w}{\partial z^2}\right) - \frac{\gamma w}{\rho_w \mathrm{K}} + g\beta(T - T_\infty) \tag{21}$$

The momentum equations for the saturated porous packed bed consist of the Brinkmann term, which describes viscous effects due to the presence of a solid body. This form of momentum equations is known as the Brinkmann-extended Darcy model [21], where γ is the dynamic viscosity, K is the medium permeability, β is the thermal expansion coefficient, α is the effective thermal diffusivity of the saturated porous packed bed, and ν is the kinematic viscosity of the fluid.

3.4 Initial and Boundary Conditions.

1. At the interface between the sample and the walls, zero slip boundary conditions are used for the momentum equations,

$$u = w = 0 \tag{22}$$

No heat exchange takes place:

$$\frac{\partial T}{\partial x} = \frac{\partial T}{\partial z} = 0 \tag{23}$$

2. The upper surface of sample exchanges with surrounding where the boundary conditions are given by

- Heat is lost from the surface via natural convection,

$$-\lambda\frac{\partial T}{\partial z} = h_c(T - T_\infty) \tag{24}$$

where h_c is the local heat transfer coefficient.

- In order to capture the real flow phenomenon, the influence of Marangoni flow is included in analyzing model where the velocity in the normal direction (w) and shear stress in the horizontal direction are assumed to be zero [15],

$$\eta\frac{\partial u}{\partial z} = -\frac{d\xi}{dT}\frac{\partial T}{\partial x} \tag{25}$$

where η and ξ are the absolute viscosity and surface tension of liquid layer, respectively.

The initial condition of the sample is defined as follows:

$$T = T_0 \quad \text{at } t = 0 \tag{26}$$

4 Numerical Procedure

Maxwell's equations (Eqs. (1)–(6)) are solved using the finite-difference time-domain (FDTD) method. The electric field components (E) are stored halfway between the basic nodes, while the magnetic field components (H) are stored at the center. So, they are calculated at alternating half-time steps. E and H field components are discretized by a central difference method (second-order accurate) in both spatial and time domains. The energy and fluid flow equations (Eqs. (17)–(21)) are solved numerically by using the finite control volume (FCV) method along with the

Table 1 Thermal and dielectric properties used in the computations [14]

Properties	Air	Water	Glass bead
$C_p(\mathrm{J/kg^{-1}\ K^{-1}})$	1007	4186	800
$\lambda(\mathrm{W\ m^{-1}\ K^{-1}})$	0.0262	0.609	1.4
$\rho(\mathrm{kg/m^{-3}})$	1.205	1000	2500
μ_r	1.0	1.0	1.0
ε_r	1.0	$88.15-0.414T+(0.131\times10^{-2})T^2-(0.046\times10^{-4})T^3$	5.1
$\tan\delta$	0.0	$0.323-(9.499\times10^{-3})T+(1.27\times10^{-4})T^2-(6.13\times10^{-7})T^3$	0.01

SIMPLE algorithm developed by Patankar [22]. These equations are coupled to Maxwell's equations by Eq. (9). Because the dielectric properties of most liquids depend on temperature, it is necessary to consider the coupling between the E field and the temperature distribution. For this reason, the iteration scheme (reference from Ratanedecho et al. [15]) is used to resolve the nonlinear coupling of Maxwell's equations, momentum, and energy equations. Spatial and temporal resolutions are selected to ensure stability and accuracy. To ensure stability of the time-stepping algorithm, Δt is chosen to satisfy the courant stability condition [15]:

$$\Delta t \le \frac{\sqrt{(\Delta x)^2+(\Delta z)^2}}{\upsilon} \tag{27}$$

The spatial resolution of each cell is defined as follows:

$$\Delta x,\Delta z \le \frac{\lambda_g}{10\sqrt{\varepsilon_r}} \tag{28}$$

The calculation conditions that correspond to Eqs. (27) and (28) are as follows:

1. Grid size: $\Delta x=1.0922$ mm and $\Delta z=1.0000$ mm
2. Time steps: $\Delta t=2\times10^{-12}$ s and $\Delta t=0.01$ s are used corresponding to electromagnetic field and temperature field calculations, respectively.
3. The relative error in the iteration procedures of 10^{-6} is chosen.

5 Results and Discussion

5.1 Physical Properties. Two samples are simulated in order to illustrate microwave heating phenomena using a rectangular waveguide with a resonator. Saturated porous packed bed and water layer are selected for this purpose. Thermal properties and temperature-dependent dielectric properties of the samples are shown in Table 1 [14]. The dielectric properties of samples are assumed independent of the microwave frequency.

The convection heat transfer coefficient $h_c=10\ \mathrm{W\ m^{-2}\ K^{-1}}$ is due to natural convection flux at the upper surface of the sample. Initially, the whole calculation domain is assumed to be at a uniform temperature of 301 K.

The penetration depth (D_p) is defined as the distance at which the power density has decreased to 37% of its initial value at the surface [20]:

$$D_p=\frac{1}{\dfrac{2\pi f}{\upsilon}\sqrt{\dfrac{\varepsilon_r'\left[\sqrt{1+\left(\dfrac{\varepsilon_r''}{\varepsilon_r'}\right)^2}-1\right]}{2}}}$$

$$=\frac{1}{\dfrac{2\pi f}{\upsilon}\sqrt{\dfrac{\varepsilon_r'[\sqrt{1+(\tan\delta)^2}-1]}{2}}} \tag{29}$$

5.2 Numerical Validations. The numerical results have been validated with experimental data of an earlier work (Cha-um et al. [23]). Figures 2(*a*) and 2(*b*) show a comparison of the numerical results and experimental data of temperature profiles along x- and z-axes, respectively (Cha-um et al. [23]). It may be noted that the earlier work was investigated without a resonator inside a rectangular waveguide. It was observed that the trends of results are in good agreement. From Fig. 2, the magnitudes of the temperatures predicted within the water layer are all close to the experimental values. Only small discrepancies are noticed. These maybe resulted from keeping some of thermal properties constant during the simulation process. For the saturated porous medium, the experimental data are significantly higher than the computational

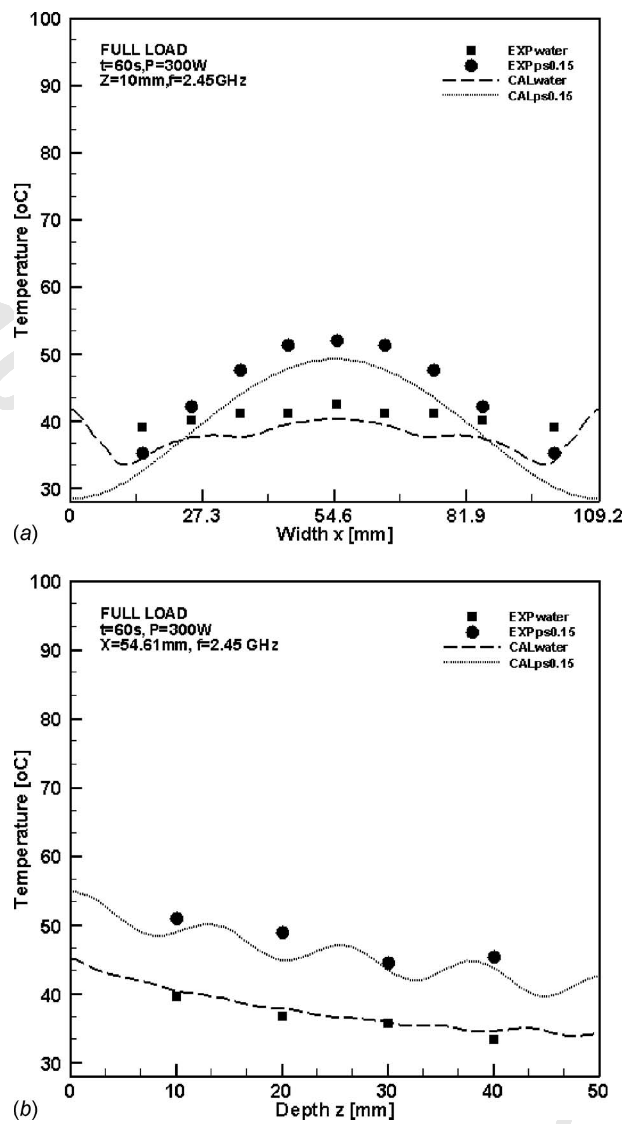

Fig. 2 Comparison of numerical solutions with experimental results of temperature profile: (*a*) along *x*-axis and (*b*) along *z*-axis

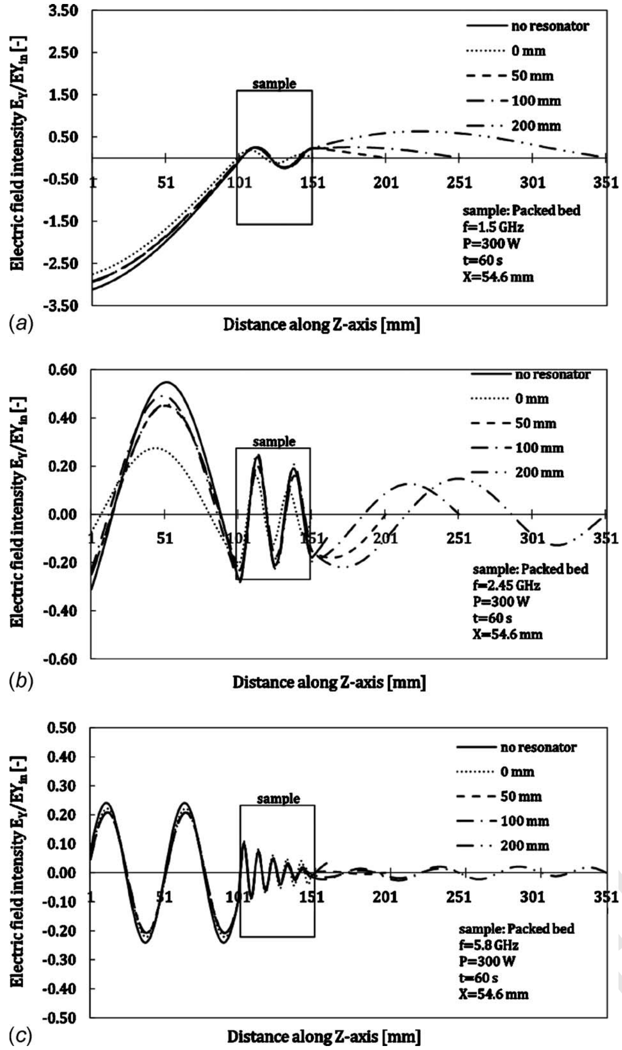

Fig. 3 Distribution of electric field within saturated packed beds filled the guide for various microwave frequencies at $t=60$ s: (*a*) 1.5 GHz, (*b*) 2.45 GHz, and (*c*) 5.8 GHz

results, especially along with the X-direction [23]. The discrepancy may be attributed to the uncertainties in some parameter such as porosity, (ϕ), and the thermal and dielectric property database. Further, the uncertainty in temperature measurement might come from the error in the measured microwave power input where the calculated uncertainty associated with temperature was less than 2.65% [23]. From this result, it is clear that the model can be used as a real tool for investigating in detail this particular microwave heating of dielectric materials at a fundamental level.

5.3 Heating Characteristics for Saturated Porous Packed Bed. This section is performed to examine the heating characteristic of a guide loaded with a saturated porous packed bed (cross section area of 109.2×54.6 mm^2) with a thickness of 50 mm.

5.3.1 Electric Field Distribution. Figure 3 illustrates the electric field distribution along the center axis ($x=54.6$ mm) of a rectangular waveguide at $t=60$ s for various resonator distances away from the right boundary at the different operating frequencies. In the figure, the vertical axis represents the intensity of the electric fields E_Y, which is normalized to the amplitude of the input electric fields E_{Yin}. In the case without a resonator, all transmitted waves through the sample are absorbed by a fixed water load at the end of the guide. For the cases with a resonator in the waveguide for various distances (0 mm, 50 mm, 100 mm, and 200 mm) and various frequencies (1.5 GHz, 2.45 GHz, and 5.8 GHz), the electric fields with a small amplitude are formed within the saturated porous packed bed, while the stronger standing wave outside the saturated porous packed bed (left-hand side) with a larger amplitude is formed by interference between the forward waves and the reflected waves from the resonator. At 2.45 GHz, the penetration depth of microwave within the saturated porous packed bed is about 110.2 mm (Table 2), which is much greater than the thickness of the saturated porous packed bed, so a large portion of the microwave is able to penetrate through the layer. However, due to the reflections occurring at the air-resonator interface, the standing wave can be formed at the right-hand side, as seen in the figure.

Table 2 Penetration depth of saturated packed bed and water (28°C)

Frequency, f (GHz)	Penetration depth, D_p (mm)	
	Saturated packed bed	Water
1.50	181.0	50.6
2.45	110.2	31.0
5.80	46.8	13.1

5.3.2 Temperature Profiles and Velocity Fields. Figure 4 illustrates the distribution of temperature within a saturated porous packed bed along depth ($x=54.6$ mm) for $t=60$ s with various resonator distances and various operating frequencies. It is shown that the highest temperature occurs at the surface and slightly decreases along the depth of the sample according to the penetration depth of microwave. For the operating frequencies of 1.5 GHz and 2.45 GHz, the penetration depths of microwave are 181.0 mm and 110.2 mm, respectively, which are larger than the thickness of a saturated porous packed bed (50 mm). Thus, the microwave can either transmit through or reflect from the resonator. The standing waves are formed and transmitted back into the saturated porous packed bed. During the 1.5 GHz operating frequency, the temperature is much higher for the case of resonator distances corresponding to 0 mm. This result indicates that the waves resonate very well, thereby forming a strong standing wave. During the 2.45 GHz operating frequency, it is interesting that the temperature is greater for the case of resonator distances at about 100 mm, whereas the saturated porous packed bed with resonator distances at 0 mm corresponds to the lowest temperature during microwave heating. While the operating frequency is 5.8 GHz, all cases correspond to lower temperature situations. Since the penetration depth of microwave within a saturated porous packed bed is about 46.8 mm, which is smaller than the thickness of the sample (50 mm), energy dissipates quickly inside the bed. Consequently, a very minimal resonance of standing wave occurs. Refer to the uniformity of temperature within the saturated porous packed bed and the temperature difference between the upper and lower surfaces for each operating frequency in Fig. 4; it is observed that the uniformity does not follow the maximum temperature. For 1.5 GHz and 2.45 GHz, the uniformity in temperature occurs for a case of no resonator and a case with resonator at a distance of about 0 mm, respectively. While the operating frequency is 5.8 GHz, it cannot be indicated because all cases correspond to same situations. Contours of temperature and velocity fields within the sample for the maximum temperature case with various operating frequencies are shown in Figs. 5 and 6, respectively. The temperature distributions qualitatively follow electric field distribution and velocity field. The flow pattern displays circulation patterns, which are characterized by the two symmetrical vortices stemming from the upper corners. The fluid flows as it is driven by the effect of buoyancy. This effect is distributed from the upper corner near the surface where the incident wave propa-

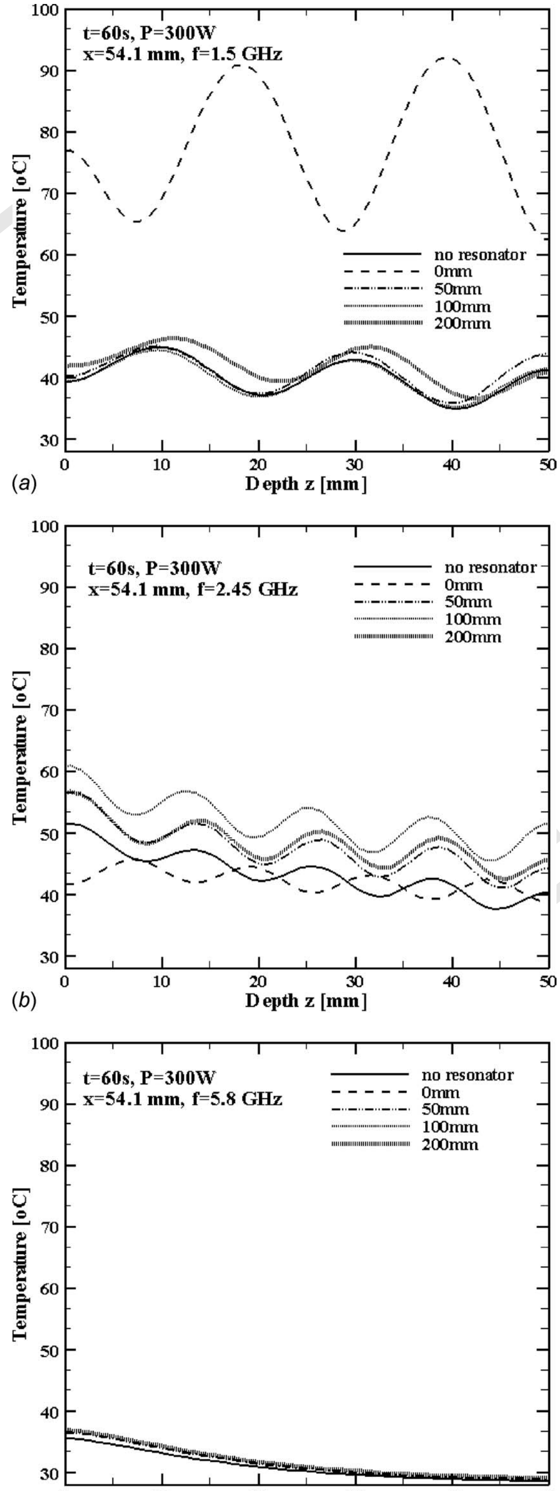

Fig. 4 Temperature profile along *z*-axis within saturated packed beds filled the guide for various microwave frequencies at $t=60$ s: (*a*) 1.5 GHz, (*b*) 2.45 GHz, and (*c*) 5.8 GHz

gates through. The buoyancy effect is associated with the lateral temperature gradient at locations near the top surface. Heated portions of the fluid become lighter than the rest of the fluid and are expanded laterally away from the sides to the center of the sample.

5.4 Heating Characteristics for Water Layer. This section presents the heating characteristics of a water layer filled in a rectangular waveguide. The sample has a 109.2×54.6 mm^2 cross section area with 30 mm of thickness.

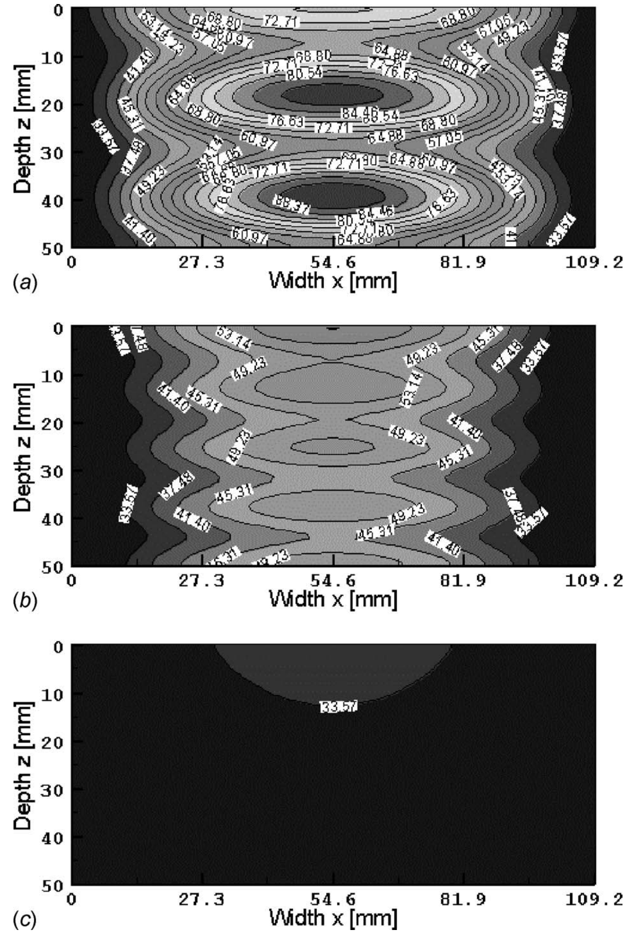

Fig. 5 Temperature contour within packed beds at 60 s: (*a*) 1.5 GHz, 0 mm; (*b*) 2.45 GHz, 100 mm; and (*c*) 5.8 GHz, 200 mm

5.4.1 Electric Fields Distribution. Figure 7 illustrates the electric field distribution along the center axis ($x=54.6$ mm) of a rectangular waveguide at $t=60$ s for various resonator distances and operating frequencies. In the figure, the vertical axis represents the intensity of the electric fields E_Y, which is normalized to the amplitude of the input electric fields E_{Yin}. From the figure, the results are similar to cases of a saturated porous packed bed. The amplitude of the electric fields is high over the surface of a water layer (left-hand side) and almost disappears within the water layer. Small amplitude transmitted waves (right-hand side) are reflected from a resonator and are transmitted back into a water layer. Note that the amplitude of electric fields within a water layer is lower than cases of the saturated porous packed bed, but the amplitude of electric fields on the surface (left-hand side) is higher than the case of the saturated porous packed bed. This is because of the small penetration depth and dielectric properties of the water layer (as seen in Tables 1 and 2).

5.4.2 Temperature Profiles and Velocity Fields. Figure 8 illustrates the distribution of temperature within a water layer along the depth ($x=54.6$ mm) for $t=60$ s with various resonator distances and various operating frequencies. It shows no significant temperature difference between surface and inside the water layer for a variety of resonator distances because the small penetration depth and convection play an important role in smoothing out the temperature profile. For 1.5 GHz and 2.45 GHz of operating fre-

PROOF COPY [HT-10-1420] 017101JHR

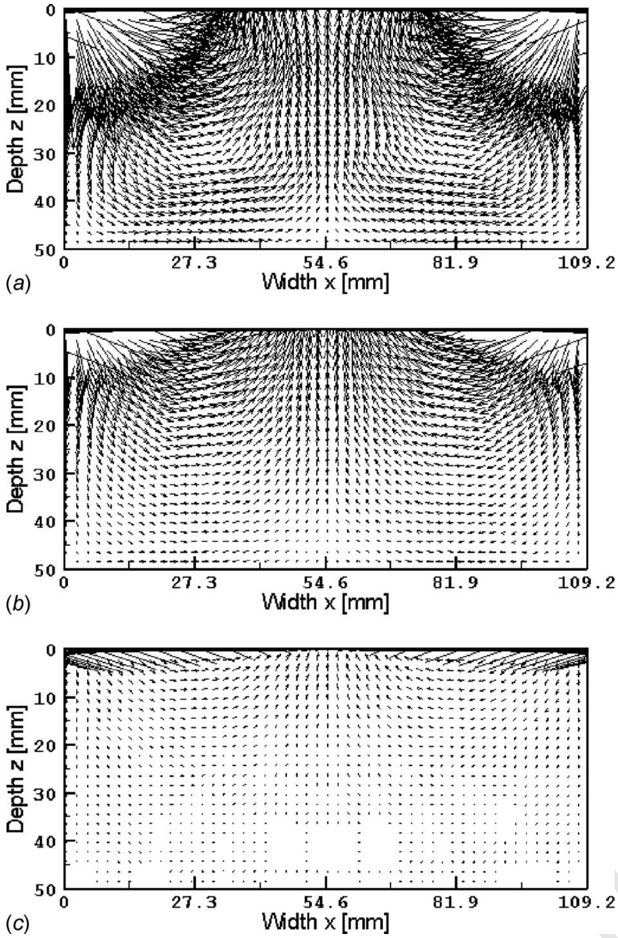

Fig. 6 Velocity field within packed beds at 60 s: (*a*) 1.5 GHz, 0 mm; (*b*) 2.45 GHz, 100 mm; and (*c*) 5.8 GHz, 200 mm (vector length (relative): 35,900,000 grid units/magnitude)

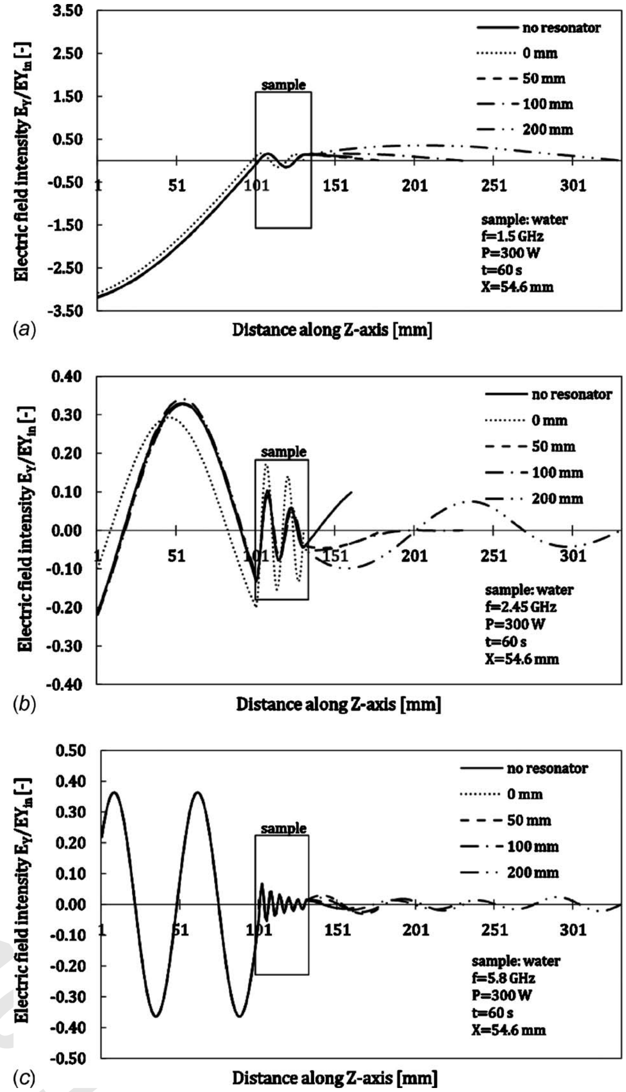

Fig. 7 Distribution of electric field within water filled the guide for various microwave frequencies at $t=60$ s: (*a*) 1.5 GHz, (*b*) 2.45 GHz, and (*c*) 5.8 GHz

quencies, the guide with resonator at a distance of 0 mm corresponds to relatively higher temperature during microwave heating. For a 5.8 GHz operating frequency, the penetration depth of microwave inside the water layer is 13.1 mm (Table 2). It is shorter than the thickness of the water layer, so all cases with and without a resonator are found to be low and give nearly the same temperature. In other words, the resonator does not affect temperature distribution when the penetration depth is lower than the thickness of the water layer since the electric field is rapidly converted to thermal energy within the water layer. The result of the uniformity of temperature is not different in each case. Figures 9 and 10 show the contour of temperature and velocity fields, respectively, within the sample for the maximum temperature case with various times and various operating frequencies. It is interesting to observe that the highest temperature is in the upper region of the heating water layer with the temperature decreasing toward the lower boundary. The velocity fields within the water layer on the x-z plane correspond to temperature fields in Fig. 9. The effect of conduction plays a greater role than convection at the early stage of heating. As the heating proceeds, the local heating on the surface water layer causes the difference of surface tension on the surface of water layer, which leads to the convective flow of water (Marangoni flow). This causes water to flow from the hot region (higher power absorbed) at the central region of the water layer to the colder region (lower power absorbed) at the sidewall of the container. In the stage of heating ($t=60$ s), the effect of convective flow becomes stronger and plays a more important role, especially at the upper portion of the sidewalls of the container. However, at the bottom region of the walls where the convection flow is small, temperature distributions are primarily governed by the conduction mode.

5.5 Comparison of Heating Characteristics: Saturated Porous Packed Bed Versus Water Layer. In this section, we highlight the microwave heating characteristics of the saturated porous packed bed and the water layer to emphasize the importance of the penetration depth of microwave and the inserted resonator. The electric field distribution, temperature profile, and velocity field show the strong function of the penetration depth of microwave within the samples (water layer (30 mm of thickness) or the saturated porous packed bed (50 mm of thickness)). The dielectric properties are temperature-dependent. Water layer is a high lossy material, but a saturated porous packed bed is a low lossy material. For all cases of operating frequencies for the saturated porous packed bed, temperature distribution is found to be larger than that for the water layer for all cases of resonator distances. For example, the maximum temperature (T) for the saturated porous packed bed with resonator distances at 0 mm is 53°C, corresponding to a 1.5 GHz operating frequency, whereas T for the water layer with resonator distances at 0 mm is 53°C, corresponding to a 1.5 GHz operating frequency ($t=40$ s, $z=30$ mm). It

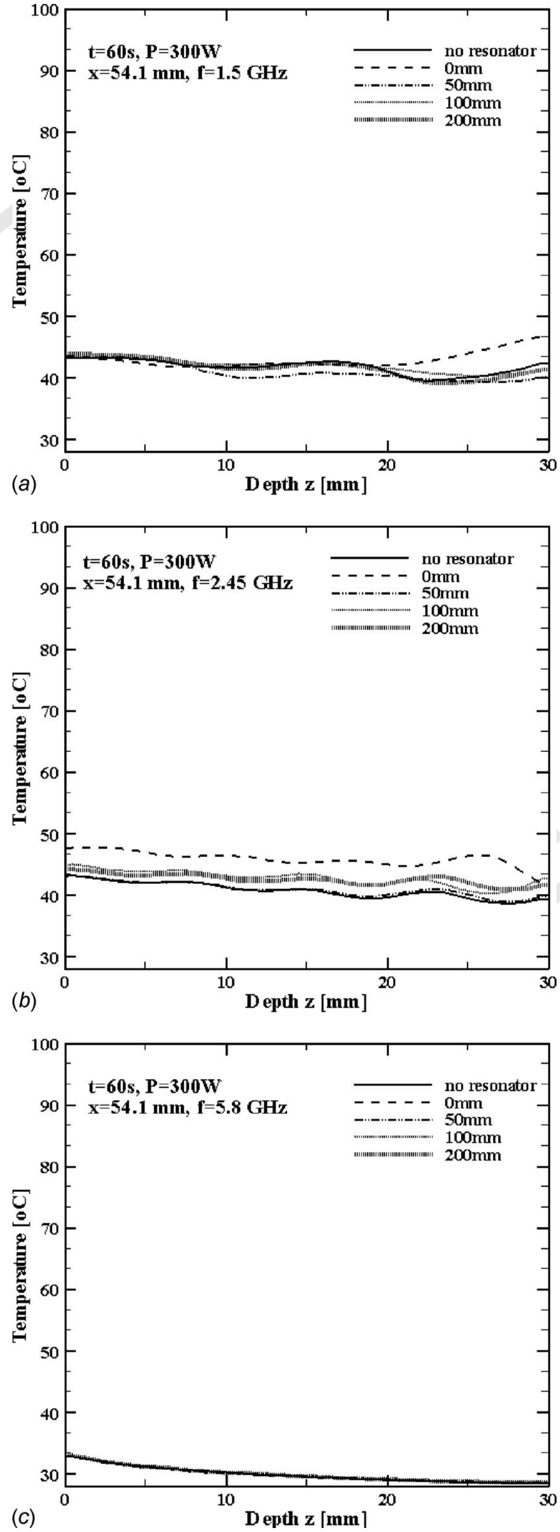

Fig. 8 Temperature profiles within water layer at 60 s: (*a*) 1.5 GHz, (*b*) 2.45 GHz, and (c) 5.8 GHz

may also be noted that greater power absorption occurs within the saturated porous packed bed than within the water layer for all cases. This is because of the standing waves formed by reflected waves from the resonator inside the saturated porous packed bed.

6 Conclusions

This paper presents the simulations of microwave heating of a saturated porous packed bed and a water layer that is filled in the guide with a resonator. The dielectric properties of the sample are found to depend strongly on temperature. The results show an interaction between physical parameters (resonator distances, operating frequencies, and dielectric properties) and microwave heating phenomena. For heating of the saturated porous packed bed, the inserted resonator strongly affects the uniformity of temperature distribution because the penetration depth of microwave is larger than the thickness of the saturated porous packed bed. The microwaves can transmit through the bed and then reflect back in the bed, forming a standing wave within the bed. For heating of water, the inserted resonator does not affect the unifor-

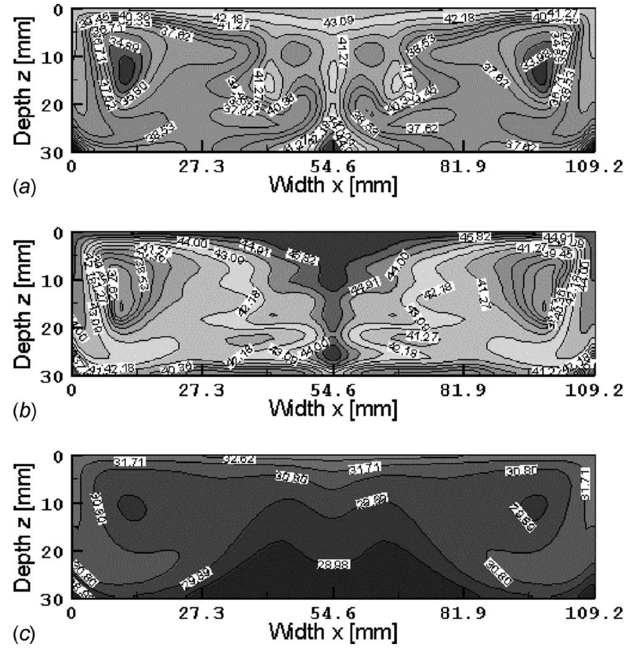

Fig. 9 Temperature contour within water layer at 60 s: (*a*) 1.5 GHz, 0 mm; (*b*) 2.45 GHz, 0 mm; and (*c*) 5.8 GHz, 200 mm

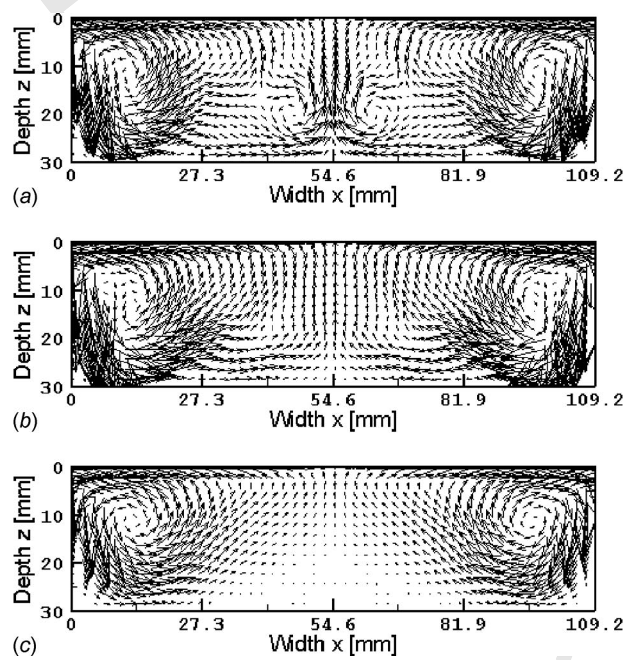

Fig. 10 Velocity field within water layer at 60 s: (*a*) 1.5 GHz, 0 mm; (*b*) 2.45 GHz, 0 mm; and (*c*) 5.8 GHz, 200 mm (vector length (relative): 2500 grid units/magnitude)

Table 3 The generalized heating strategies for saturated packed bed and water layer

	Saturated packed bed ($109.2\times54.6\times50$ mm^3)		Water layer ($109.2\times54.6\times30$ mm^3)	
Heating strategy (GHz)	Maximum temperature (mm)	Uniform temperature (mm)	Maximum temperature (mm)	Uniform temperature (mm)
1.5	0	No resonator	0	Nonsignificant
2.45	100	0	0	Nonsignificant
5.8	200	Nonsignificant	Nonsignificant	Nonsignificant

mity of temperature distribution except for the case of operating frequency at 1.5 GHz because the penetration depth of microwave during 1.5 GHz is larger than the thickness of the water layer. Additionally, the convection mode plays a significant role on heat transfer in the water layer.

Table 3 illustrates the heating characteristics for both the saturated porous packed bed and the water layer for various operating frequencies without a resonator and with a resonator at different distances. It is observed that the case with a resonator distance of 0 mm may be the optimal choice for the high heating rate saturated porous packed bed with 1.5 GHz and for the water layer with 2.45 GHz, while no obvious benefit when using a resonator is observed in the other cases. However, Table 3 provides some useful guidelines for optimal microwave heating of a saturated porous packed bed and a water layer with a resonator inserted in the guide.

Acknowledgment

The authors gratefully acknowledge the financial support provided by The Thailand Research Fund for the simulation facilities described in this paper.

Nomenclature

C_p = specific heat capacity J/(kg K)
E = electric field intensity (V/m)
f = frequency of incident wave (Hz)
g = gravitational constant (m/s^2)
H = magnetic field intensity (A/m)
p = pressure (Pa)
P = power (W)
Q = local electromagnetic heat generation term (W/m^3)
s = Poynting vector (W/m^2)
t = time (s)
T = temperature (°C)
$\tan\delta$ = dielectric loss coefficient
u,w = velocity component (m/s)
Z_H = wave impedance (Ω)
Z_l = intrinsic impedance (Ω)

Greek Letters

α = thermal diffusivity (m^2/s)
β = coefficient of thermal expansion (1/K)
γ = dynamic viscosity (Pa/s)
ε = permittivity (F/m)
η = absolute viscosity (Pa s)
λ = wavelength (m)
μ = magnetic permeability (H/m)
ν = kinematics viscosity (m^2/s)
ξ = surface tension (N/m)
ρ = density (kg/m^3)
σ = electric conductivity (S/m)
υ = velocity of propagation (m/s)
ω = angular frequency (rad/s)

Subscripts

∞ = ambient condition
a = air
j = layer number
in = input
w = water
p = particle

References

[1] Ayappa, K. G., Davis, H. T., Crapiste, G., Davis, E. A., and Gordon, J., 1991, "Microwave Heating: An Evaluation of Power Formulations," Chem. Eng. Sci., **46**(4), pp. 1005–1016.
[2] Ayappa, K. G., Davis, H. T., Davis, E. A., and Gordon, J., 1992, "Two-Dimensional Finite Element Analysis of Microwave Heating," AIChE J., **38**(10), pp. 1577–1592.
[3] Datta, A. K., Prosetya, H., and Hu, W., 1992, "Mathematical Modeling of Batch Heating of Liquids in a Microwave Cavity," J. Microwave Power Electromagn. Energy, **27**, pp. 38–48.
[4] Jia, X., and Bialkowski, M., 1992, "Simulation of Microwave Field and Power Distribution in a Cavity by a Three Dimension Finite Element Method," J. Microwave Power Electromagn. Energy, **27**(1), pp. 11–22.
[5] Liu, F., Turner, I., and Bialowski, M., 1994, "A Finite-Difference Time-Domain Simulation of Power Density Distribution in a Dielectric Loaded Microwave Cavity," J. Microwave Power Electromagn. Energy, **29**(3), pp. 138–147.
[6] Ayappa, K. G., Brandon, S., Derby, J. J., Davis, H. T., and Davis, E. A., 1994, "Microwave Driven Convection in a Square Cavity," AIChE J., **40**(7), pp. 1268–1272.
[7] Zhang, Q., Jackson, T. H., and Ungan, A., 2000, "Numerical Modeling of Microwave Induced Natural Convection," Int. J. Heat Mass Transfer, **43**, pp. 2141–2154.
[8] Clemens, J., and Saltiel, C., 1996, "Numerical Modeling of Materials Processing in Microwave Furnaces," Int. J. Heat Mass Transfer, **39**(8), pp. 1665–1675.
[9] Chatterjee, S., Basak, T., and Das, S. K., 2007, "Microwave Driven Convection in a Rotating Cylindrical Cavity: A Numerical Study," J. Food. Eng., **79**, pp. 1269–1279.
[10] Zhu, J., Kuznetsov, A. V., and Sandeep, K. P., 2007, "Mathematical Modeling of Continuous Flow Microwave Heating of Liquid (Effect of Dielectric Properties and Design Parameters)," Int. J. Therm. Sci., **46**, pp. 328–341.
[11] Zhu, J., Kuznetsov, A. V., and Sandeep, K. P., 2007, "Numerical Simulation of Forced Convection in a Duct Subjected to Microwave Heating," Heat Mass Transfer, **43**, pp. 255–264.
[12] Zhu, J., Kuznetsov, A. V., and Sandeep, K. P., 2008, "Investigation of a Particulate Flow Containing Spherical Particles Subjected to Microwave Heating," Heat and Mass Transfer, **44**, pp. 481–493.
[13] Zhu, J., Kuznetsov, A. V., and Sandeep, K. P., 2007, "Numerical Modeling of a Moving Particle in a Continuous Flow Subjected to Microwave Heating," Numer. Heat Transfer, Part A, **52**, pp. 417–439.
[14] Rattanadecho, P., Aoki, K., and Akahori, M., 2001, "A Numerical and Experimental Study of Microwave Drying Using a Rectangular Waveguide," Drying Technology An International Journal , **19**(9), pp. 2209–2234.
[15] Ratanadecho, P., Aoki, K., and Akahori, M., 2002, "A Numerical and Experimental Investigation of the Modeling of Microwave Heating for Liquid Layers Using a Rectangular Waveguide (Effects of Natural Convection and Dielectric Properties)," Appl. Math. Model., **26**(3), pp. 449–472.
[16] Rattanadecho, P., Aoki, K., and Akahori, M., 2002, "Experimental Validation of a Combined Electromagnetic and Thermal Model for a Microwave Heating of Multi-Layered Materials Using a Rectangular Waveguide," ASME J. Heat Transfer, **124**(5), pp. 992–996.
[17] Rattanadecho, P., 2006, "The Simulation of Microwave Heating of Wood Using a Rectangular Wave Guide: Influence of Frequency and Sample Size," Chem. Eng. Sci., **61**(14), pp. 4798–4811.
[18] Curet, S., Rouaud, O., and Boillereaux, L., 2008, "Microwave Tempering and Heating a Single-Mode Cavity: Numerical and Experimental Investigations," Chem. Eng. Process., **47**, pp. 1656–1665.
[19] Tada, S., Echigo, R., and Yoshida, H., 1998, "Numerical Analysis of Electromagnetic Wave in a Partially Loaded Microwave Applicator," Int. J. Heat

Mass Transfer, **41**, pp. 709–718.

[20] Basak, T., Aparna, K., Meenakshi, A., and Balakrishnan, A. R., 2006, "Effect of Ceramic Supports on Microwave Processing of Porous Food Samples," Int. J. Heat Mass Transfer, **49**, pp. 4325–4339.

[21] Pakdee, W., and Rattanadecho, P., 2006, "Unsteady Effects on Natural Convective Heat Transfer Through Porous Media in Cavity Due to Top Surface Partial Convection," Appl. Therm. Eng., **26**(17–18), pp. 2316–2326.

[22] Patankar, S. V., 1980, *Numerical Heat Transfer and Fluid Flow*, Henisphere, New York.

[23] Cha-um, W., Pakdee, W., and Rattanadecho, P., 2009, "Experimental Analysis of Microwave Heating of Dielectric Materials Using a Rectangular Wave Guide (MODE:TE_{10}) (Case Study: Water Layer and Saturated Porous Medium)," Exp. Therm. Fluid Sci., **33**(3), pp. 472–481.

[24] Cha-um, W., Rattanadecho, P., and Pakdee, W., 2009, "Experimental and Numerical Analysis of Microwave Heating of Water and Oil Using a Rectangular Wave Guide: Influence of Sample Sizes, Positions, and Microwave Power," Food Bioprocess Technol., in press.10.1007/s11947-009-0187-x

[25] Metaxas, A. C., and Meridith, R. J., 1983, *Industrial Microwave Heating*, Peter Peregrinus, London.

[26] Vafai, K., 2005, "General Characteristics and Modeling of Porous Media," *Handbook of Porous Media*, Taylor & Francis, NW London, Chap. I.

PROOF COPY [HT-10-1420] 017101JHR

AUTHOR QUERIES — 017101JHR

#1 Au: All references must be cited in text, in numerical order. Please cite Refs. 24–26 in text.